

Orbits in the Field of a Gravitating Magnetic Monopole

Valeria Kagramanova¹, Jutta Kunz¹ and Claus Lämmerzahl²

¹ Institut für Physik, Universität Oldenburg, D–26111 Oldenburg, Germany

² ZARM, Universität Bremen, Am Fallturm, D–28359 Bremen, Germany

July 1, 2021

Abstract

Orbits of test particles and light rays are an important tool to study the properties of space–time metrics. Here we systematically study the properties of the gravitational field of a globally regular magnetic monopole in terms of the geodesics of test particles and light. The gravitational field depends on two dimensionless parameters, defined as ratios of the characteristic mass scales present. For critical values of these parameters the resulting metric coefficients develop a singular behavior, which has profound influence on the properties of the resulting space–time and which is clearly reflected in the orbits of the test particles and light rays.

PACS:

1 Introduction

To understand the properties of classical solutions of the gravitational field equations it is essential to study the orbits of test particles and light rays in these space–times. On the one hand, this is important from an observational point of view, since it is only matter and light that is observed and that therefore can give insight into a given gravitational field [1]. The study of the motion of test particles in gravitational fields has thus significant practical applications. On the other hand, this study is also important from a fundamental point of view, since the motion of matter and light can be used to classify a given space–time, to decode its structure and to highlight its characteristics.

Particles and light have been used since a long time to discuss the properties of solutions of Einstein’s field equations. All solutions of the geodesic equation in a Schwarzschild gravitational field can be found in a seminal paper of Hagihara [2]. With the same mathematical tools one can solve the geodesic equation in a Reissner–Nordström space–time [3]. The analytic solutions of the geodesic equation in a Kerr and Kerr–Newman space–time are also known (see [3] for a survey). Analytic solutions are the starting point for approximation methods for the description of real stellar, planetary, comet, asteroid, or satellite trajectories (see e.g. [4]). Analytic solutions of the geodesic equation can also serve as test beds for numerical codes for the dynamics of binary systems in the extreme stellar mass ratio case and also for the calculation of corresponding gravitational wave templates.

Here we discuss orbits in a static spherically symmetric gravitational field, where the space–time metric is expressed in terms of Schwarzschild–like coordinates,

$$ds^2 = g_{tt}dt^2 + g_{rr}dr^2 + r^2(d\vartheta^2 + \sin^2\vartheta d\varphi^2). \quad (1)$$

We further assume, that the space–time is asymptotically flat. Well-known examples of such space–times are the Schwarzschild solution and the Reissner–Nordström solution, both representing black hole solutions with an event horizon and a central singularity. In these solutions, the two metric coefficients are not independent, but related to each other, $g_{tt}g_{rr} = -1$. At the event horizon $g_{rr} \rightarrow \infty$, while the curvature invariants remain finite. At the origin, in contrast, the curvature invariants diverge, indicating the presence of a classical singularity.

When matter fields other than the Maxwell field are coupled to gravity, not only black hole solutions arise but globally regular solutions can appear as well. Interesting examples of such globally regular solutions

of the coupled Einstein-matter field equations are boson stars, which form when a scalar field is coupled to gravity, or magnetic monopoles, which originate in grand unified theories. These solutions neither possess an event horizon nor a central singularity. Their curvature invariants are finite everywhere, and the two metric functions no longer satisfy the relation $g_{tt}g_{rr} = -1$, instead $g_{tt}g_{rr} = -A(r)$.

Our interest here focuses on orbits of test particles and light rays in such space-times, and, in particular, in space-times emerging in the presence of globally regular magnetic monopoles [5, 6] as described in Section 4. Magnetic monopoles arise as topological defects in theories which undergo spontaneous symmetry breaking. In general, magnetic monopoles exist if the mapping of the vacuum manifold, associated with the symmetry breaking, onto the two-sphere is non-trivial. The existence of magnetic monopoles is consequently a generic prediction of grand unification. If magnetic monopoles were indeed present in the universe, they would have a host of astrophysical and cosmological consequences. One might even think of calculating the form of gravitational waves created by scattering processes at such monopole solutions, since these may contribute to a stochastic gravitational wave background emerging in the very early universe.

For magnetic monopoles the Einstein-matter equations depend on two dimensionless parameters, which represent ratios of the characteristic mass scales present in the theory. Depending on the values of these two parameters, the metric coefficients g_{tt} and g_{rr} can exhibit an interesting behaviour: the component g_{tt} then approaches zero within a certain domain, $0 \leq r \leq r_0$, while g_{rr} tends to infinity at the special value r_0 , and remains finite elsewhere [6]. We here demonstrate, that this intriguing behavior is clearly reflected in the particle orbits. (When one considers SU(2) Einstein-Yang-Mills theory without Higgs fields, also globally regular configurations result [7]. These solutions are unstable [8], however, and this makes them less attractive to study orbits in their vicinity.)

In Section 2 we recall the general set of equations of motion for test particles and light rays and also discuss the effective potential. We then review a number of physical quantities relevant for the interpretation of the orbits of the test particles and light rays and discuss the general features of singular limits of the metric functions in Section 3. In Section 4 we recall the basic equations and main properties of gravitating non-Abelian magnetic monopoles. In Section 5, the main section of the paper, we then present numerical results obtained for the possible types of orbits in the gravitational field of a magnetic monopole. We here exhibit the trajectories of test particles and light rays together with their proper time resp. affine parameter, and we emphasize the peculiar features of the orbits, which arise for *almost* critical values of the parameters. We give our conclusions in Section 6.

2 Equations of motion and effective potential

2.1 Equations of motion

We briefly recall the equations of motion for test particles and light in the general static spherically symmetric metric, Eq. (1). Because of spherical symmetry, one can restrict the motion to the equatorial plane. One obtains two constants of motion, the specific energy E and the specific angular momentum L (i.e., energy and angular momentum per unit mass for a particle),

$$E = -g_{tt} \frac{dt}{d\tau}, \quad (2)$$

$$L = r^2 \frac{d\varphi}{d\tau}, \quad (3)$$

where for particles τ is the proper time, while for light it represents an affine parameter. Then the only dynamical equation left is

$$\left(\frac{dr}{d\tau}\right)^2 = -\left(\frac{E^2}{g_{tt}g_{rr}} + \frac{1}{g_{rr}}\left(\epsilon + \frac{L^2}{r^2}\right)\right), \quad (4a)$$

where $\epsilon = 1$ for particles and $\epsilon = 0$ for light. Exploiting energy and angular momentum conservation one obtains the equations for φ and t as functions of r

$$\left(\frac{dr}{d\varphi}\right)^2 = -\frac{r^4}{L^2} \left(\frac{E^2}{g_{tt}g_{rr}} + \frac{1}{g_{rr}} \left(\epsilon + \frac{L^2}{r^2} \right) \right), \quad (5a)$$

$$\left(\frac{dr}{dt}\right)^2 = -\frac{g_{tt}^2}{E^2} \left(\frac{E^2}{g_{tt}g_{rr}} + \frac{1}{g_{rr}} \left(\epsilon + \frac{L^2}{r^2} \right) \right). \quad (5b)$$

Eqs. (4a)-(5b) then give a complete description of the dynamics. From Eq. (4a) it is clear that the motion is restricted to the domain $E^2 + g_{tt} \left(\epsilon + \frac{L^2}{r^2} \right) \geq 0$.

2.2 Effective potential

When reasoning by analogy to the Newtonian case [9], a natural definition arises for an effective potential of the Schwarzschild space–time from the geodesic equation. For the general asymptotically flat case we are discussing here, no such natural definition is available. Therefore we propose a set of conditions which we consider to be natural properties of an effective potential, and which in our case are sufficient to give a unique definition for an effective potential.

We thus suggest that an effective potential U_{eff} for an asymptotically flat space–time should possess the following properties:

1. The effective potential should determine the equation of motion for the r -coordinate: $\frac{d^2r}{d\tau^2} = -\frac{dU_{\text{eff}}}{dr}$.
2. The effective potential should obey the boundary condition $\lim_{r \rightarrow \infty} U_{\text{eff}}(r) = 0$.

The first condition leads to

$$\frac{1}{2} \left(\frac{dr}{d\tau} \right)^2 = \mathcal{E} - U_{\text{eff}}, \quad (6)$$

where \mathcal{E} is a constant. To fix this constant we decompose the two metric functions g_{tt} and g_{rr} according to

$$\frac{1}{g_{tt}(r)} = -1 - f_{tt}(r), \quad \frac{1}{g_{rr}(r)} = 1 + f_{rr}(r), \quad (7)$$

where $\lim_{r \rightarrow \infty} f_{tt}(r) = 0$ and $\lim_{r \rightarrow \infty} f_{rr}(r) = 0$, in accordance with asymptotic flatness, and we also exploit the second condition. The equation for the radial motion Eq. (4a) then becomes

$$\begin{aligned} \frac{1}{2} \left(\frac{dr}{d\tau} \right)^2 &= \frac{1}{2} (1 + f_{tt}(r)) (1 + f_{rr}(r)) E^2 - \frac{1}{2} (1 + f_{rr}(r)) \left(\epsilon + \frac{L^2}{r^2} \right) \\ &= \frac{E^2 - \epsilon}{2} + \frac{1}{2} (f_{tt}(r) + f_{rr}(r) + f_{tt}(r)f_{rr}(r)) E^2 - \frac{\epsilon}{2} f_{rr}(r) - (1 + f_{rr}(r)) \frac{L^2}{2r^2}. \end{aligned} \quad (8)$$

Except for the first term all other terms tend to zero for $r \rightarrow \infty$, so that we can make the unique identification

$$\begin{aligned} \mathcal{E} &= \frac{E^2 - \epsilon}{2}, \quad U_{\text{eff}} = -\frac{1}{2} (f_{tt}(r) + f_{rr}(r) + f_{tt}(r)f_{rr}(r)) E^2 + \frac{\epsilon}{2} f_{rr}(r) + (1 + f_{rr}(r)) \frac{L^2}{2r^2} \\ &= \frac{1}{2} \left(E^2 - \epsilon + \frac{E^2}{g_{tt}g_{rr}} + \frac{1}{g_{rr}} \left(\epsilon + \frac{L^2}{r^2} \right) \right). \end{aligned} \quad (9)$$

Thus in general the effective potential depends on both constants of motion, on L and on E .

Since the right hand side of Eq. (8) is quadratic in E , one can recast the equation in the form [10]

$$\frac{1}{2} \left(\frac{dr}{d\tau} \right)^2 = \frac{1}{2} (1 + f_{tt}(r)) (1 + f_{rr}(r)) (E^2 - U(r)) = -\frac{1}{2} \frac{E^2 - U(r)}{g_{tt}(r)g_{rr}(r)}, \quad (10)$$

and identify the quantity U ,

$$U = \frac{\epsilon + \frac{L^2}{r^2}}{1 + f_{tt}(r)} = -g_{tt}(r) \left(\epsilon + \frac{L^2}{r^2} \right), \quad (11)$$

where $U(r) \rightarrow \epsilon$ for $r \rightarrow \infty$. Although U is sometimes called an effective potential, it is not an effective potential in the sense of the above criteria. However, U has the big advantage of being independent of the energy E , and from

$$E^2 - U(r) = 0 \quad (12)$$

one can easily determine the values of r , which mark the turning points and thus give the range of the motion. Thus the range of the motion of particles and light is most easily obtained from U and independent of E . However, the full features of the geodesics are obtained only from U_{eff} and are dependent on E .

3 Properties of orbits

For the subsequent discussion of the orbits in the space–time of a magnetic monopole it is instructive to first recall a number of physical properties relevant for the description of the motion. These are the proper time, the physical distance and the physical velocity.

We then discuss the limiting features of a metric, when the metric coefficients g_{tt} and g_{rr} tend to zero or diverge. The curvature invariants here indicate the presence of a mere coordinate singularity or of a physical singularity. We first address these limits for the Schwarzschild and Reissner–Nordström solutions, where $g_{tt}g_{rr} = -1$. Then we turn to the more general case, realized in the space–time of a gravitating magnetic monopole, where $g_{tt}g_{rr} = -A(r)$. Here our statements about the limits should be interpreted to only mean “very small” and “very large”. The treatment of the limits in the strict mathematical sense will be discussed in a subsequent publication [11].

These considerations are then used in Section 5 in order to obtain an interpretation of the calculated trajectories. They may be also of relevance, when one considers a “splitting” of space–time or a space–time “without time”, features which might occur in generalized models of gravity.

3.1 Proper time

An important feature of the motion of a particle is the proper time elapsing along its trajectory. Along a radial trajectory, e.g., the proper time is given by

$$\tau - \tau_0 = \int_{\tau_0}^{\tau} d\tau = \int_{r_0}^r \frac{d\tau}{dr} dr = \int_{r_0}^r \left(-\frac{E^2}{g_{tt}g_{rr}} - \frac{1}{g_{rr}} \left(\epsilon + \frac{L^2}{r^2} \right) \right)^{-\frac{1}{2}} dr. \quad (13)$$

Now if a whole region arises in a space–time, where g_{tt} is very small ($g_{tt} \rightarrow 0$), as in the case of the nearly critical space–times of a magnetic monopole, then in such a region $\frac{d\tau}{dr}$ is very small as well ($\frac{d\tau}{dr} \rightarrow 0$). This means, that a particle does not feel anything like a singularity in such a region, but that it simply needs almost no proper time to traverse such a region.

3.2 Proper distance

Another relevant physical quantity is the distance as measured from the origin in a regular region of space–time,

$$l = \int_0^r \sqrt{g_{rr}} dr. \quad (14)$$

When $g_{rr} \rightarrow \infty$ at some coordinate value r_0 , the distance to r_0 becomes infinite, if $\sqrt{g_{rr}}$ is not integrable at r_0 . The space–time in the region $0 \leq r \leq r_0$ then has infinite extent.

3.3 Physical velocity

The velocity dr/dt in Eq. (5b) is the coordinate velocity and not a physical velocity. A physical velocity is measured, e.g., by an observer at rest in the given coordinate system. The proper time of such an observer at r is given by $dT = -\sqrt{g_{tt}}dt$, and the physical distance to the origin (in a regular space–time) has been defined in Eq. (14). The radial velocity measured by such an observer at rest then is

$$v = \frac{dl}{dT} = \sqrt{\frac{g_{rr}}{-g_{tt}}} \frac{dr}{dt}. \quad (15)$$

With the geodesic equation Eq. (5b) this yields for the measured velocity

$$v = \sqrt{\frac{g_{rr}}{-g_{tt}} \frac{1}{|E|} \sqrt{\frac{-g_{tt}}{g_{rr}} \sqrt{E^2 + g_{tt} \left(\epsilon + \frac{L^2}{r^2} \right)}}} = \sqrt{1 + \frac{g_{tt}}{E^2} \left(\epsilon + \frac{L^2}{r^2} \right)}. \quad (16)$$

The measured velocity is well defined in the allowed regions of the motion, which are restricted by the requirement of positivity of the radicand. Clearly, the measured velocity of a particle is always limited by the velocity of light. For $\epsilon = 0$ the measured velocity is the light velocity. We note, that the velocity measured by an observer at rest does not depend on g_{rr} .

3.4 Curvature invariants

To differentiate between mere coordinate singularities and physical singularities it is instructive to consider the curvature invariants. The simplest of these invariants is the Kretschmann scalar $K = R_{\mu\nu\rho\sigma}R^{\mu\nu\rho\sigma}$. For the static spherically symmetric metric Eq. (1) the Kretschmann scalar is given by

$$\begin{aligned} K = & \frac{4}{r^4} \left(1 - \frac{1}{g_{rr}} \right)^2 + \frac{1}{4g_{rr}^2} \left(2\frac{g_{tt}''}{g_{tt}} - \left(\frac{g_{tt}'}{g_{tt}} \right)^2 \right)^2 + \frac{2}{r^2 g_{rr}^2} \left(\frac{g_{tt}'}{g_{tt}} \right)^2 \\ & + \frac{1}{2g_{rr}^2} \frac{g_{rr}'}{g_{rr}} \left(\frac{g_{tt}'}{g_{tt}} \right)^3 - \frac{1}{g_{rr}^2} \frac{g_{tt}''}{g_{tt}} \frac{g_{tt}'}{g_{tt}} \frac{g_{rr}'}{g_{rr}} + \frac{1}{4g_{rr}^2} \left(\frac{g_{tt}'}{g_{tt}} \right)^2 \left(\frac{g_{rr}'}{g_{rr}} \right)^2 + \frac{2}{r^2 g_{rr}^2} \left(\frac{g_{rr}'}{g_{rr}} \right)^2. \end{aligned} \quad (17)$$

In the Schwarzschild and Reissner-Nordström solutions, for instance, the Kretschmann scalar remains finite at the horizons, whereas it diverges at the classical physical singularities at the origin.

3.5 Equations of motion for *almost singular metric coefficients*

The equations of motion Eqs. (4a)-(5b) depend on the metric coefficients. The equations for $dr/d\varphi$ and $dr/d\tau$ depend on the metric coefficient g_{rr} , and on the product $g_{tt}g_{rr}$, while the equation for dr/dt further contains the factor g_{tt} .

To address the effects of *almost singular metric coefficients* on the orbits of particles and light, we here distinguish two cases. In the first case, we consider space-times, where the metric coefficients satisfy the relation $g_{tt}g_{rr} = -1$, such as, e.g., the black hole space-times of the Schwarzschild metric and the Reissner-Nordström metric.

In the second case we consider globally regular asymptotically flat metrics, where the metric coefficients are constrained by the above relation only at spatial infinity, thus $g_{tt}g_{rr} = -A(r)$ with $\lim_{r \rightarrow \infty} A(r) = 1$. These metrics include the generic space-time of a magnetic monopole (see section 4). When certain critical values of the coupling constants are approached, such a globally regular space-time may, however, evolve towards a space-time with singular metric coefficients, possibly associated with physical singularities. Studying the orbits of particles and light is expected to yield a deeper understanding of such limiting space-times.

3.5.1 $g_{tt}g_{rr} = -1$

When $g_{tt}g_{rr} = -1$, as, e.g., in the Schwarzschild and Reissner-Nordström solutions, the equations of motion reduce to

$$\left(\frac{dr}{d\varphi} \right)^2 = \frac{r^4}{L^2} \left(E^2 - \frac{1}{g_{rr}} \left(\epsilon + \frac{L^2}{r^2} \right) \right), \quad (18a)$$

$$\left(\frac{dr}{d\tau} \right)^2 = E^2 - \frac{1}{g_{rr}} \left(\epsilon + \frac{L^2}{r^2} \right), \quad (18b)$$

$$\left(\frac{dr}{dt} \right)^2 = \frac{g_{rr}^2}{E^2} \left(E^2 - \frac{1}{g_{rr}} \left(\epsilon + \frac{L^2}{r^2} \right) \right). \quad (18c)$$

We now consider a number of effects relevant for the orbits, which arise when g_{rr} becomes very small or very large, as collected in the following Table:

	$g_{rr} \rightarrow 0$	$g_{rr} \rightarrow \infty$
$\frac{dr}{d\varphi}$	needs $E \rightarrow \infty$	$E^2 \frac{r^4}{L^2}$
$\frac{dr}{ds}$	needs $E \rightarrow \infty$	E^2
$\frac{dr}{dt}$	$\rightarrow \infty$ (provided E is large enough)	$\rightarrow 0$
$d\tau$	0	finite/infinite*
v	$\sqrt{1 - \frac{1}{E^2 g_{rr}} \left(\epsilon + \frac{L^2}{r^2} \right)}$ (provided E is large enough)	$\sqrt{1 - \frac{1}{E^2 g_{rr}} \left(\epsilon + \frac{L^2}{r^2} \right)}$

* depending on whether Eq. (13) is integrable or not

When $g_{rr} \rightarrow \pm\infty$ ($g_{tt} \rightarrow 0$) at some coordinate value r_0 , a horizon is encountered, as, e.g., in the Schwarzschild and Reissner–Nordström space–times. The coordinate r then changes from space–like to time–like or vice versa, unless the horizon is degenerate as in the case of an extremal Reissner–Nordström black hole.

For $g_{rr} \rightarrow 0$ ($g_{tt} \rightarrow \pm\infty$) on the other hand, a singularity is approached in, e.g., the Schwarzschild and Reissner–Nordström space–times. When $g_{rr} > 0$, motion is allowed only in the region close to the singularity, if the energy is large enough to compensate for the large negative second term in the equations (proportional to $1/g_{rr}$). The vanishing of $d\tau$ (or the finiteness of τ) indicates a finite proper time along a geodesic, which is a standard criterion for the occurrence of a singularity [12].

3.5.2 $g_{tt}g_{rr} = -A(r)$

This case is formulated to be applicable to the motion of particles and light in the gravitational field of a magnetic monopole, to be discussed below. The two metric functions are now constrained by the relation $g_{tt}g_{rr} = -1$ only at spatial infinity, while elsewhere their product corresponds to an independent function, $g_{tt}g_{rr} = -A(r)$, determined by the Einstein–matter equations.

We now consider the effects relevant for the orbits, which arise when g_{tt} and/or g_{rr} become very small or very large:

	$g_{tt} \rightarrow 0$	$g_{tt} \rightarrow -\infty$	$g_{rr} \rightarrow 0$	$g_{rr} \rightarrow \infty$
$\frac{dr}{d\varphi}$	$\rightarrow \infty$	$\rightarrow -\frac{r^4}{L^2 g_{rr}} \left(\epsilon + \frac{L^2}{r^2} \right)$	$\rightarrow \infty$	$\rightarrow 0$
$\frac{dr}{d\tau}$	$\rightarrow \infty$	$\rightarrow -\frac{1}{g_{rr}} \left(\epsilon + \frac{L^2}{r^2} \right)$	$\rightarrow \infty$	$\rightarrow 0$
$\frac{dr}{dt}$	$\rightarrow 0$	$\rightarrow \infty$	$\rightarrow \infty$	$\rightarrow 0$
$d\tau$	0	finite	0	finite/infinite*
v	1	requires large E	$\sqrt{1 + \frac{g_{tt}}{E^2} \left(\epsilon + \frac{L^2}{r^2} \right)}$	$\sqrt{1 + \frac{g_{tt}}{E^2} \left(\epsilon + \frac{L^2}{r^2} \right)}$

* depending on whether Eq. (13) is integrable or not

1. When $g_{tt} \rightarrow 0$, this may
 - a) occur at a specific coordinate value r_0 , and then signal the presence of a horizon, when it is associated with $g_{rr} \rightarrow \pm\infty$.
 - b) occur within a whole region of space–time, where $g_{rr} > 0$. The radial distance then changes very fast for small variations of the angle. Therefore a particle crosses such a region on quasi radially straight lines.
2. When $g_{tt} \rightarrow -\infty$, the traversed coordinate range is always finite, while the coordinate velocity tends to become large. The latter can be understood since in this case it needs a very small t to generate a large proper time.
3. When $g_{rr} \rightarrow 0$, particles need to cover a huge coordinate range in order to move a certain proper distance. That means that r has to become very large and, thus, all quantities proportional to dr become very large.
4. When $g_{rr} \rightarrow \infty$ at a specific coordinate value r_0 ,
 - a) a horizon is encountered, when at the same time $g_{tt} \rightarrow 0$. The coordinate velocity goes to zero, such that the particle appears to be no longer able to move and cross the point r_0 .
 - b) a singularity may arise, leading to a split of space–time.

4 The gravitating non-Abelian monopole

In order to be able to discuss the motion of particles and light in the gravitational field of a magnetic monopole, we now briefly recall the basic equations and the main features of the monopole space–times.

4.1 Action

$SU(2)$ Einstein–Yang–Mills–Higgs theory is described by the action

$$S = \int \left\{ \frac{R}{16\pi G} - \frac{1}{2} \text{Tr} (F_{\mu\nu} F^{\mu\nu}) - \frac{1}{4} \text{Tr} (D_\mu \Phi D^\mu \Phi) - \frac{\lambda}{4} \text{Tr} [(\Phi^2 - v^2)^2] \right\} \sqrt{-g} d^4x, \quad (19)$$

with curvature scalar R , $su(2)$ field strength tensor

$$F_{\mu\nu} = \partial_\mu A_\nu - \partial_\nu A_\mu + ie[A_\mu, A_\nu], \quad (20)$$

gauge potential $A_\mu = A_\mu^a \tau^a / 2$, and covariant derivative of the Higgs field $\Phi = \Phi^a \tau^a$ in the adjoint representation

$$D_\mu \Phi = \partial_\mu \Phi + ie[A_\mu, \Phi]. \quad (21)$$

Here G and e denote the gravitational and gauge coupling constants, respectively, v denotes the vacuum expectation value of the Higgs field, and λ represents the strength of the Higgs self-coupling.

The nonzero vacuum expectation value of the Higgs field breaks the non-Abelian $SU(2)$ gauge symmetry to an Abelian $U(1)$ symmetry. The particle spectrum of the theory then consists of a massless photon, two massive vector bosons of mass $M_W = ev$, and a Higgs field of mass $M_H = \sqrt{2\lambda} v$. In the limit $\lambda \rightarrow 0$ the Higgs potential vanishes, and the Higgs field becomes massless.

4.2 General equations of motion

Variation of the action Eq. (19) with respect to the metric $g^{\mu\nu}$ leads to the Einstein equations

$$G_{\mu\nu} = R_{\mu\nu} - \frac{1}{2} g_{\mu\nu} R = 8\pi G T_{\mu\nu} \quad (22)$$

with stress-energy tensor

$$\begin{aligned} T_{\mu\nu} &= 2 \text{Tr} (F_{\mu\alpha} F_{\nu\beta} g^{\alpha\beta}) - \frac{1}{4} g_{\mu\nu} F_{\alpha\beta} F^{\alpha\beta} \\ &+ \text{Tr} \left(\frac{1}{2} D_\mu \Phi D_\nu \Phi - \frac{1}{4} g_{\mu\nu} D_\alpha \Phi D^\alpha \Phi \right) - \frac{\lambda}{8} g_{\mu\nu} \text{Tr} (\Phi^2 - v^2)^2. \end{aligned} \quad (23)$$

Variation with respect to the gauge potential A_μ and the Higgs field Φ leads to the matter field equations,

$$\frac{1}{\sqrt{-g}}D_\mu(\sqrt{-g}F^{\mu\nu}) - \frac{1}{4}ie[\Phi, D^\nu\Phi] = 0 , \quad (24)$$

$$\frac{1}{\sqrt{-g}}D_\mu(\sqrt{-g}D^\mu\Phi) + \lambda(\Phi^2 - v^2)\Phi = 0 . \quad (25)$$

4.3 Ansätze

To obtain a static spherically symmetric magnetic monopole with unit magnetic charge we parametrize the metric in Schwarzschild-like coordinates [5, 6]

$$ds^2 = g_{tt}(r)dt^2 + g_{rr}(r)dr^2 + r^2(d\theta^2 + \sin^2\theta d\phi^2) , \quad (26)$$

and introduce the mass function $m(r)$

$$g_{rr}(r) = \left(1 - \frac{2m(r)}{r}\right)^{-1} . \quad (27)$$

For the gauge potential and the Higgs field we employ the spherically symmetric Ansätze [5, 6]

$$A_\mu dx^\mu = \frac{1 - K(r)}{2e} (\tau_\varphi d\theta - \tau_\theta \sin\theta d\varphi) , \quad (28)$$

and

$$\Phi = vH(r)\tau_r , \quad (29)$$

where the $su(2)$ matrices τ_r , τ_θ and τ_φ are defined as products of the spherical spatial unit vectors with the vector of Pauli matrices τ^a .

4.4 Dimensionless quantities

We now introduce the dimensionless coupling constants α and β as ratios of the mass scales present in the theory,

$$\alpha^2 = \frac{4\pi M_W^2}{g^2 M_{Pl}^2} = 4\pi Gv^2 , \quad \beta^2 = \frac{1}{2} \frac{M_H^2}{M_W^2} = \frac{\lambda}{e^2} , \quad (30)$$

and $M_{Pl} = 1/\sqrt{G}$ is the Planck mass. We further pass to dimensionless coordinates, $evr \rightarrow r$, and a dimensionless mass function, $evm \rightarrow m$.

4.5 Monopole equations of motion

The tt and rr components of the Einstein equations then yield equations for the mass function m and for the product $g_{tt}g_{rr}$,

$$m' = \alpha^2 \left(K'^2 + \frac{1}{2}r^2 H'^2 - \frac{2m}{r}K'^2 - mrH'^2 + \frac{(K^2 - 1)^2}{2r^2} + H^2 K^2 + \frac{\beta^2}{4}r^2(H^2 - 1)^2 \right) , \quad (31)$$

and

$$(g_{tt}g_{rr})' = 2\alpha^2 r \left(\frac{2K'^2}{r^2} + H'^2 \right) (g_{tt}g_{rr}) , \quad (32)$$

where the prime indicates the derivative with respect to r . For the matter functions we obtain the equations

$$\frac{1}{\sqrt{-g_{tt}g_{rr}}} \left(\frac{\sqrt{-g_{tt}g_{rr}}K'}{g_{rr}} \right)' = K \left(\frac{K^2 - 1}{r^2} + H^2 \right) , \quad (33)$$

and

$$\frac{1}{\sqrt{-g_{tt}g_{rr}}} \left(\frac{r^2 \sqrt{-g_{tt}g_{rr}} H'}{g_{rr}} \right)' = H (2K^2 + \beta^2 r^2 (H^2 - 1)) . \quad (34)$$

This set of equations depends only on the dimensionless coupling constants α and β . Since no analytic solutions to these field equations are known, we use numerical solutions for the calculation of the test particle orbits.

4.6 Boundary conditions

To obtain globally regular particle-like solutions we require at the origin the boundary conditions

$$m(0) = 0 , \quad K(0) = 1 , \quad H(0) = 0 . \quad (35)$$

Asymptotic flatness implies that the metric functions g_{tt} and g_{rr} approach constants at infinity. We adopt

$$g_{tt}(\infty)g_{rr}(\infty) = -1 . \quad (36)$$

$m(\infty)$ represents the dimensionless mass of the monopole solutions.

The matter functions satisfy asymptotically

$$K(\infty) = 0 , \quad H(\infty) = 1 . \quad (37)$$

4.7 Embedded Reissner-Nordström solutions

A special black hole solution of the set of coupled equations is the embedded Reissner-Nordström solution with unit magnetic charge,

$$m(r) = m_\infty - \frac{\alpha^2}{2r} , \quad g_{tt}(r)g_{rr}(r) = -1 , \quad (38)$$

$$K(r) = 0 , \quad H(r) = 1 . \quad (39)$$

The extremal Reissner-Nordström solution with event horizon radius r_H satisfies

$$r_H = m_\infty = \alpha . \quad (40)$$

4.8 Properties of magnetic monopole solutions

The coupling to gravity has a significant effect on the magnetic monopole solutions present in flat space [5]. When the coupling constant α is increased from zero, a branch of gravitating monopole solutions emerges smoothly from the flat space 't Hooft-Polyakov monopole solution. This branch of gravitating monopole solutions extends up to a maximal value α_{\max} , beyond which gravity becomes too strong for regular monopole solutions to persist [6].

For vanishing coupling constant β , this first gravitating monopole branch merges with a second branch at α_{\max} , which extends slightly backwards, up to a critical value α_{cr} of the coupling constant. At α_{cr} this second branch of gravitating monopole solutions bifurcates with the branch of extremal Reissner-Nordström solutions.

In particular, at $r_0 = \alpha_{\text{cr}}$ a double zero of the metric function $1/g_{rr}$ appears. But r_0 does not correspond to a degenerate horizon. The Kretschmann scalar diverges there. The exterior space-time of the solution, however, corresponds to the one of an extremal Reissner-Nordström black hole with unit magnetic charge [6]. The interior space-time retains regularity at the center, due to the influence of the non-Abelian fields present.

As β increases, the second branch decreases in size, until at a certain value of β the maximal value α_{\max} and the critical value α_{cr} coincide [6]. For a considerably larger value of β another interesting phenomenon arises. The metric function $1/g_{rr}$ develops a second minimum, and the double zero now arises at a value $r^* < r_0$, where r^* does correspond to a degenerate horizon. The critical solution then corresponds to an extremal black hole with non-Abelian hair and with a mass less than that of the corresponding extremal Reissner-Nordström solution [13].

5 Motion in the space–time of a gravitating monopole

This section constitutes the central part of the work. Here we present and discuss the possible types of orbits in the space–time of a gravitating monopole. The monopole solutions depend on the dimensionless parameters α and β . The parameters then enter via the respective metric functions in the equations of motion and determine via the potentials the allowed trajectories of particles and light.

We first address the potential U and the effective potential U_{eff} in these monopole space–times, considering, in particular, their expansion close to the origin. We then discuss the orbits of particles and light obtained numerically in these space–times. Here we exhibit generic examples of the possible types of motion, and we discuss motion in space–times very close to critical monopole solutions.

One of the interesting features of the motion in the space–time of a monopole is the capture of light rays by the source when α is big: here light is found to move on bound geodesics. Large α space–times also admit two bound regions for particles to move in.

5.1 Potentials

The space–time of a generic non-Abelian magnetic monopole is globally regular and asymptotically flat. Only when critical values of the parameters are approached the space–time may evolve coordinate or physical singularities.

Asymptotic flatness implies appropriate boundary conditions for the metric functions, which are reflected in the fall-off of the functions f_{rr} and f_{tt} , introduced in Eq. (7) to define the effective potential. From Eq. (27) we identify f_{rr} for the monopole space–time,

$$f_{rr}(r) = -\frac{2m(r)}{r} \quad (41)$$

which vanishes for $r \rightarrow \infty$. From the monopole boundary condition Eq. (36) we also infer that $f_{tt} \rightarrow 0$ for $r \rightarrow \infty$. Thus the effective potential U_{eff} has the required asymptotic behaviour.

The generic monopole space–time is globally regular, i.e., there is, in particular, no singularity present at the origin, but the space–time is smooth there. This is seen in the expansions of the metric functions at the origin, since for small r one finds [6]

$$f_{rr}(r) = -c\alpha^2 r^2 + \mathcal{O}(r^4), \quad f_{tt}(r) = c' + \mathcal{O}(r), \quad (42)$$

where c and c' are constants. It is also reflected in the smooth behaviour of the curvature invariants close to the origin.

Close to the origin, the potentials then have the following expansion

$$U_{\text{eff}} = \frac{L}{2r^2} + d + \mathcal{O}(r), \quad (43)$$

$$U = \frac{L^2}{2r^2} + \frac{d'}{r} + d'' + \mathcal{O}(r), \quad (44)$$

where d , d' , and d'' are constants. Therefore, for $r \rightarrow 0$ a repulsive angular momentum barrier is always present in the effective potential, unless the motion is purely radial. In orbits with finite angular momentum particles or light rays can never reach the origin, $r = 0$.

As in the Newtonian case, the angular momentum barrier here dominates close to origin. But while the angular momentum barrier increases with increasing L , its influence is modulated by the metric function g_{tt} , so that in regions with very small $|g_{tt}|$ the influence of the angular momentum barrier is reduced. This is seen in Fig. 1, where the potential U and the effective potential U_{eff} are shown for $(\alpha, \beta) = (0.85, 8.282558)$.

5.2 Orbits for $\beta = 0$

We now discuss the possible orbits for particles and light rays in monopole space–times at vanishing β . We begin with a set of typical solutions, obtained for $(\alpha, \beta) = (0.25, 0)$. As α is increased a maximal value α_{max} is reached, which still allows for the existence of a globally regular monopole solution. Beyond α_{max} only black hole solutions exist. We exhibit a set of typical orbits present at $\alpha_{\text{max}} = 1.403$.

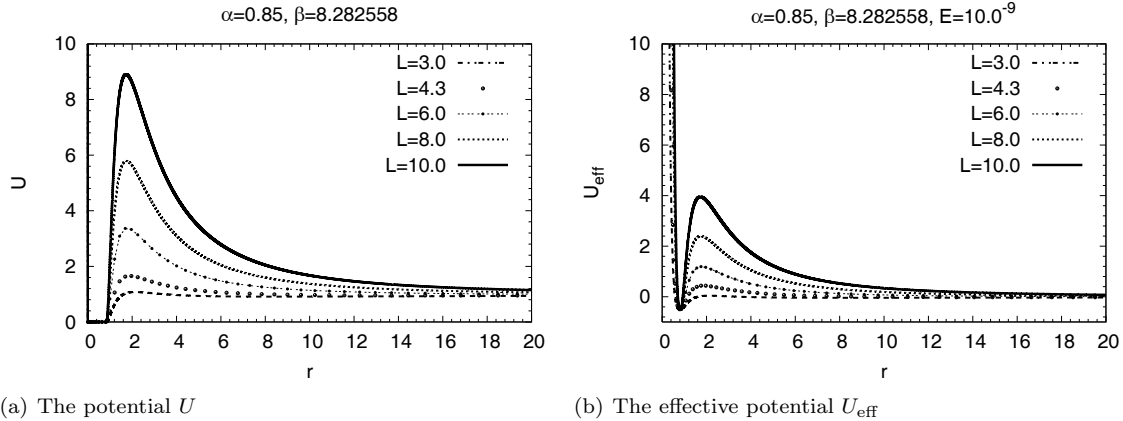


Figure 1: The potential U (a) and the effective potential U_{eff} at energy $E = 10^{-9}$ (b) versus the radial coordinate r for the parameters $(\alpha, \beta) = (0.85, 8.282558)$ and several angular momenta L (see subsection 5.3.2).

When $\beta = 0$ (or small), two regular monopole solutions exist in the range $\alpha_{\text{cr}} < \alpha \leq \alpha_{\text{max}}$. For $\beta = 0$, the critical value of α is determined to be (within numerical accuracy) $\alpha_{\text{cr}} = 1.385853$. It is called critical, because as $\alpha \rightarrow \alpha_{\text{cr}}$ the minimum of the metric function $1/g_{rr}$ decreases, and reaches zero at a certain value r_0 of the radial coordinate in the limit. The region of space-time with $r \geq r_0$ of the critical solution then corresponds to the exterior space-time of an extremal Reissner-Nordström black hole. We exhibit a set of orbits at $\alpha_{\text{cr}} = 1.385853$, i.e., for an *almost* critical space-time.

In the following we always present figures for the metric functions $-g_{tt}$ and $1/g_{rr}$, the curvature invariant K , and the potential U , and exhibit various typical and special orbits obtained for given values of the angular momentum L and the energy E .

5.2.1 Orbits at $\alpha = 0.25$

We begin with the discussion of the generic case of a monopole space-time, as exhibited in Fig. 2 for $(\alpha, \beta) = (0.25, 0)$. The metric coefficient $-g_{tt}$ has a finite value at the origin and rises monotonically to its asymptotic value, $-g_{tt}(\infty) = 1$. The metric coefficient $1/g_{rr}$ assumes the value $1/g_{rr} = 1$ both at the origin and asymptotically, and exhibits a minimum at some value of the radial coordinate, r_0 . The Kretschmann scalar is finite everywhere and small.

The potential U shows, that the orbits in such a space-time have the general structure of typical Newtonian orbits: there is one circular orbit corresponding to the minimum of U , and there are bound orbits as well as scattering states.

To exhibit the possible types of orbits, we choose as a representative value for the angular momentum, $L = 0.5$. As seen in Fig. 3, the orbits indeed show the qualitative structure inferred from U . The main difference to the typical Newtonian orbits is the occurrence of a perihelion (perimonopoleon) shift for bound orbits, showing that the underlying potential differs from the Newtonian potential of a point mass. The elapsed proper time along the orbits is also indicated.

5.2.2 Orbits at $\alpha_{\text{max}} = 1.403$

We now consider the orbits for the maximal value of α , i.e., for the parameters $(\alpha_{\text{max}}, \beta) = (1.403, 0)$. Again, the metric coefficient $-g_{tt}$ is a monotonically rising function, and the metric coefficient $1/g_{rr}$ exhibits a minimum at some value of the radial coordinate, r_0 , although the minimum is much deeper now. The Kretschmann scalar is still finite everywhere and not too large.

The most interesting feature here is that the potential U can now possess two minima and a maximum. In such a case, bound orbits are present in two distinct regions of space. We exhibit typical examples of such bound orbits in Fig. 5 for an angular momentum of $L = 4.3$. The first three figures (a), (b) and (c) show orbits in the inner region (associated with the inner minimum), for a low energy value, $E = \sqrt{0.2}$, for

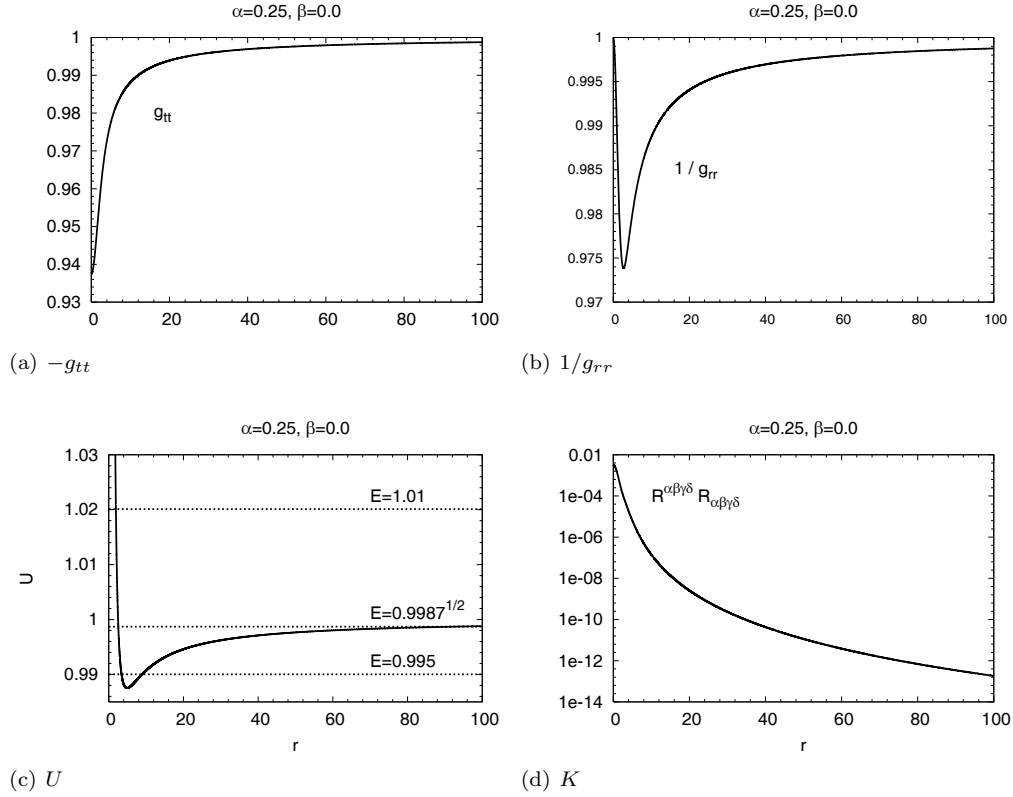


Figure 2: The metric functions $-g_{tt}$ (a) and $1/g_{rr}$ (b), the potential U (c) and the curvature invariant K (d) versus the radial coordinate r for $(\alpha, \beta) = (0.25, 0)$.

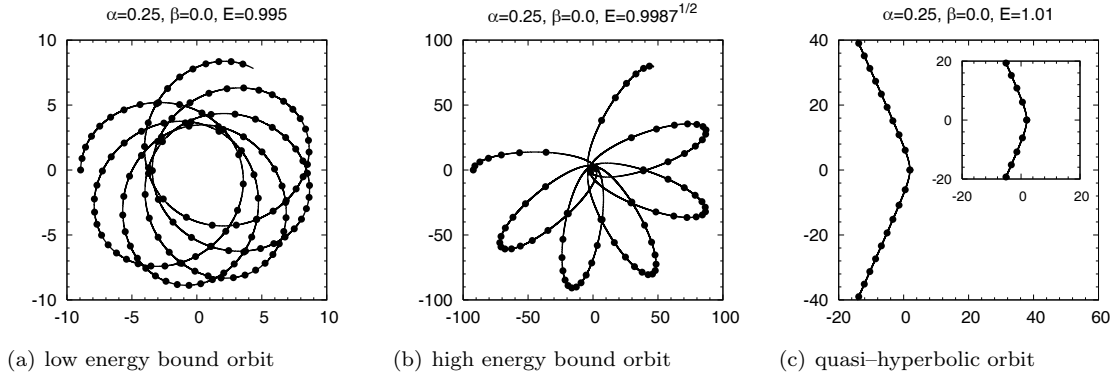


Figure 3: Particle orbits $r(\varphi)$ for $(\alpha, \beta) = (0.25, 0)$. The dots indicate units of elapsed proper time.

a higher energy value, $E = \sqrt{0.5}$, and for the (all but) highest value possible for a bound orbit in the inner region, $E = \sqrt{0.908}$.

For very low energies the orbits of course approach a circular orbit. As the energy increases, the orbits have a deformed shape, and show a very pronounced perihelion shift ((a) and (b)). When the limiting energy value E_{\max} for bound orbital motion in the inner region is approached, the associated unstable circular orbit becomes apparent, since it forms the outer envelope of the trajectory (c).

In the energy interval between the outer minimum and the maximum, there are orbits in the inner region

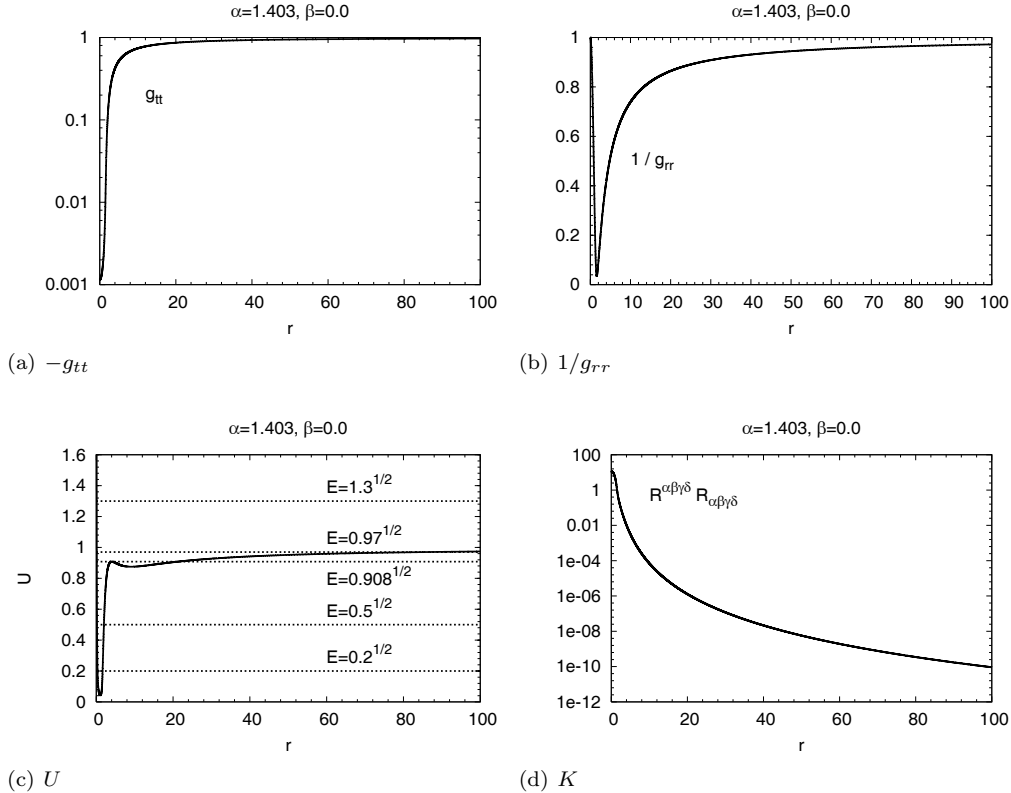


Figure 4: The metric functions $-g_{tt}$ (a) and $1/g_{rr}$ (b), the potential U (c) and the curvature invariant K (d) versus the radial coordinate r for $(\alpha_{\max}, \beta) = (1.403, 0)$.

(c) as well as in the outer region (d). Here the unstable circular orbit associated with the maximum becomes apparent as the inner boundary for the orbital motion. For still higher energies, in the range $E_{\max} < E < 1$ one observes quasi-elliptic orbits (e). In the outer region these look like ellipses. When they get close to the inner region, the unstable circular orbit is again reflected in the motion, but it no longer forms a boundary. Instead the motion proceeds further inwards, orbits close to the center and then proceeds outwards again, as highlighted in the inset of (e).

For energies $E > 1$, we observe scattering states (f). The particle then encircles the central region several times (twice in (f)) before escaping into infinity again.

5.2.3 Orbits at $\alpha_{\text{cr}} = 1.38585$

We now demonstrate, how the monopole space-time evolves as the critical solution is approached. As $\alpha \rightarrow \alpha_{\text{cr}}$ the minimum of the metric function $1/g_{rr}$ decreases and reaches zero in the limit. This decrease towards zero is seen in Fig. 6. Note, that α_{cr} is here determined only within a certain numerical accuracy, and therefore the final solution obtained is only *almost* critical: $1/g_{rr}$ does not yet fully reach zero at some coordinate value r_0 , but it is extremely small there.

The true limiting solution then consists of two parts: the interior region $0 \leq r < r_0$ and the exterior region $r_0 < r < \infty$. Since the limiting exterior solution corresponds to an extremal Reissner–Nordström space-time, $r_0 = \alpha$ must hold for the limiting solution, according to Eq. (40). The limiting interior solution is in a non-Abelian solution and regular at the origin.

As $\alpha \rightarrow \alpha_{\text{cr}}$ the metric function $-g_{tt}$ becomes increasingly small in the inner region, $0 \leq r < r_0$, tending to zero in the limit. Close to r_0 , however, $-g_{tt}$ rises very steeply to assume its asymptotic value of one, as imposed by the boundary conditions. In the limit $\alpha \rightarrow \alpha_{\text{cr}}$, $-g_{tt}$ appears to become singular at r_0 .

The emergence of a singularity at r_0 is also indicated by the Kretschmann scalar of the monopole space-time, which appears to diverge in the limit. In contrast, the Kretschmann scalar of the associated extremal Reissner–Nordström black hole remains finite at its degenerate horizon r_0 , but diverges for $r \rightarrow 0$, as seen in

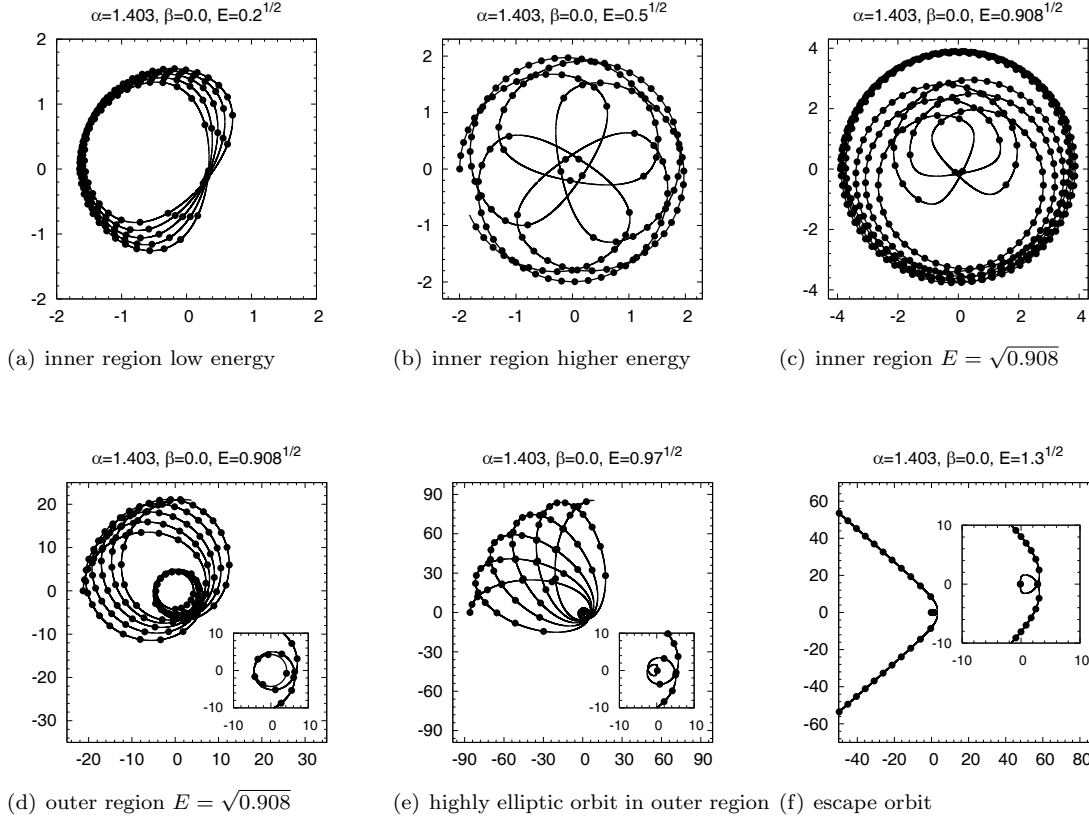


Figure 5: Particle orbits $r(\varphi)$ for $(\alpha_{\max}, \beta) = (1.403, 0)$. The crosses indicate units of elapsed proper time.

Fig. 6.

Let us now consider the motion of particles in the *almost* critical space–time, with parameters $(\alpha, \beta) = (1.38585, 0)$, and exemplify the intriguing effects of this *almost* critical space–time on the orbital motion. We study the orbits for a representative value of the angular momentum, $L = 4.3$. As shown in Fig. 6, the potential U then again possesses two minima. We therefore expect the same general types of orbits as in the previous case.

We display a set of characteristic orbits in Fig. 7. The bound orbits in the inner region (a) and (b) (connected to the inner minimum of the potential) are now hugely distorted as compared to ordinary bound orbits. In the energy interval between the outer minimum and the maximum, bound orbits are present in the inner (c) as well as in the outer region (d). Again the unstable circular orbit associated with the maximum becomes apparent as the outer envelope of the allowed motion in the inner region (c) and as the inner boundary for the trajectories in the outer region (d). For still higher energies, in the range $E_{\max} < E < 1$ we again observe quasi-elliptic orbits with additional inner loops circling the center (e), while for energies $E > 1$, we again observe scattering states (f).

The most surprising feature is the deformation of the orbits in the inner region. As seen in Fig. 6, the orbits evolve smoothly until they reach the vicinity of the critical value of the radial coordinate, r_0 . There they abruptly change direction and approach in almost straight radial lines the center. Very close to the center they are reflected (passing partial arcs), and then move outwards again in almost straight radial lines, until they reach the vicinity of r_0 , where they again abruptly change direction.

This intriguing pattern of movement can be understood as follows: for $r < r_0$ the effective potential very quickly tends to extremely large negative values, as seen in Fig. 6. Therefore in this region a particle is vigorously attracted towards the origin. This huge attraction leads to orbits which are almost straight radial lines. (Note, that this interpretation is related to the first column of the table in subsection 3.5.2.) The

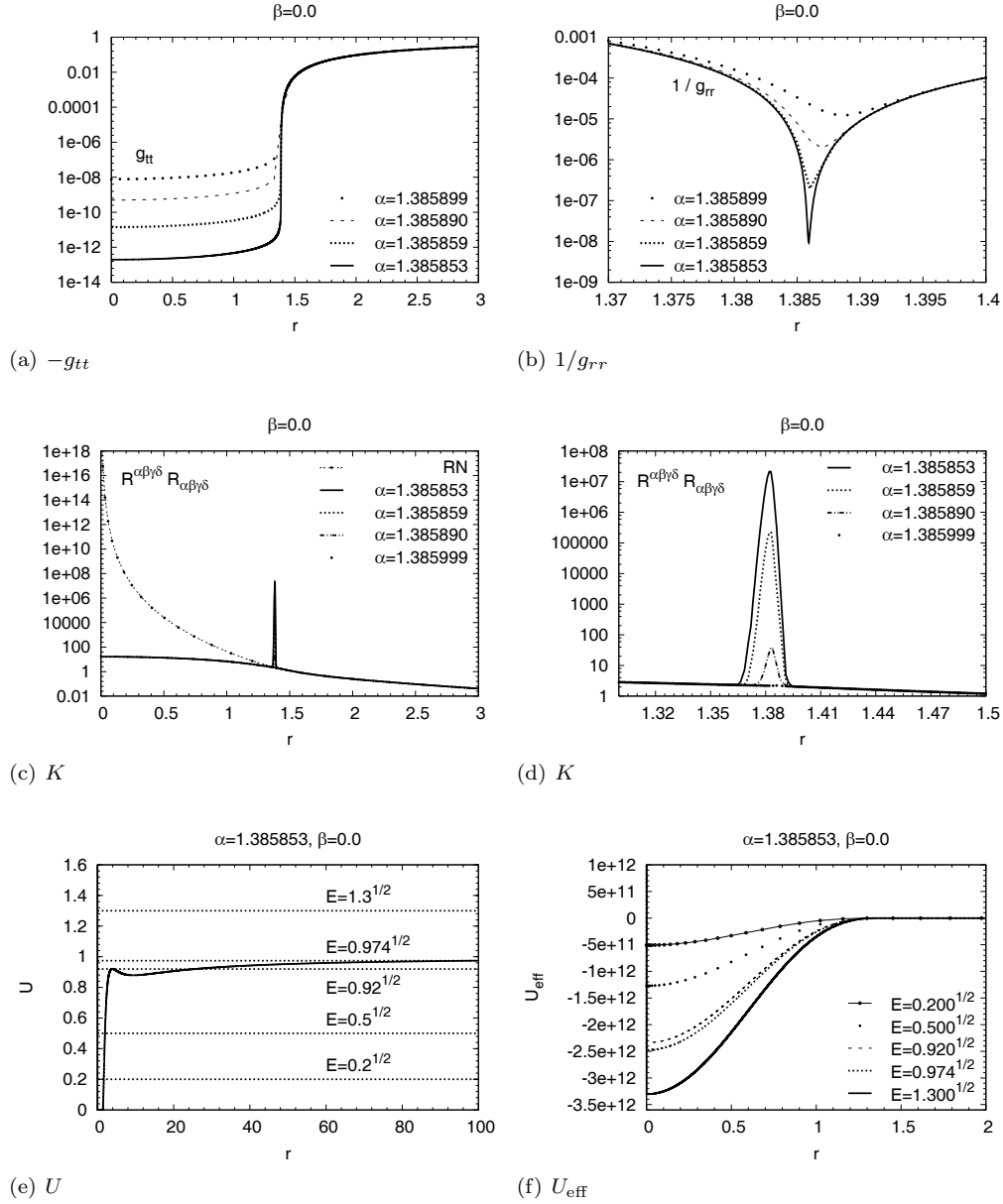


Figure 6: The metric functions $-g_{tt}$ (a) and $1/g_{rr}$ (b), the curvature invariant K (c) and (d), the potential U (e), and the effective potential U_{eff} (f), versus the radial coordinate r for $(\alpha_{\text{cr}}, \beta) = (1.38585, 0)$. (RN denotes the extremal Reissner–Nordström black hole.)

deflection close to the center is caused by the potential barrier there.

Interesting is also a glance at the proper time of a particle along these almost straight radial parts of the orbits. Since $-g_{tt}$ is extremely small, a particle needs almost no proper time to traverse the inner region, as exemplified in Fig. 6 (and also discussed in subsection 3.5.2).

Let us finally consider these orbits in terms of the proper distance l instead of the radial coordinate r . In Fig. 8 we exhibit the dependence $l(r)$ for a sequence of solutions approaching the critical solution. The figure demonstrates, that the space–time develops a throat, as $\alpha \rightarrow \alpha_{\text{cr}}$. In the limit, the throat becomes infinitely long [6]. For the *almost* critical value $\alpha = 1.385853$, l grows already by a factor of 20 in the vicinity of r_0 .

The rapid growth of l in the vicinity of r_0 has significant influence on the shape of the orbits. The abrupt directional changes seen in the orbits $r(\varphi)$ in the vicinity of r_0 are smoothed out, when $l(\varphi)$ is considered

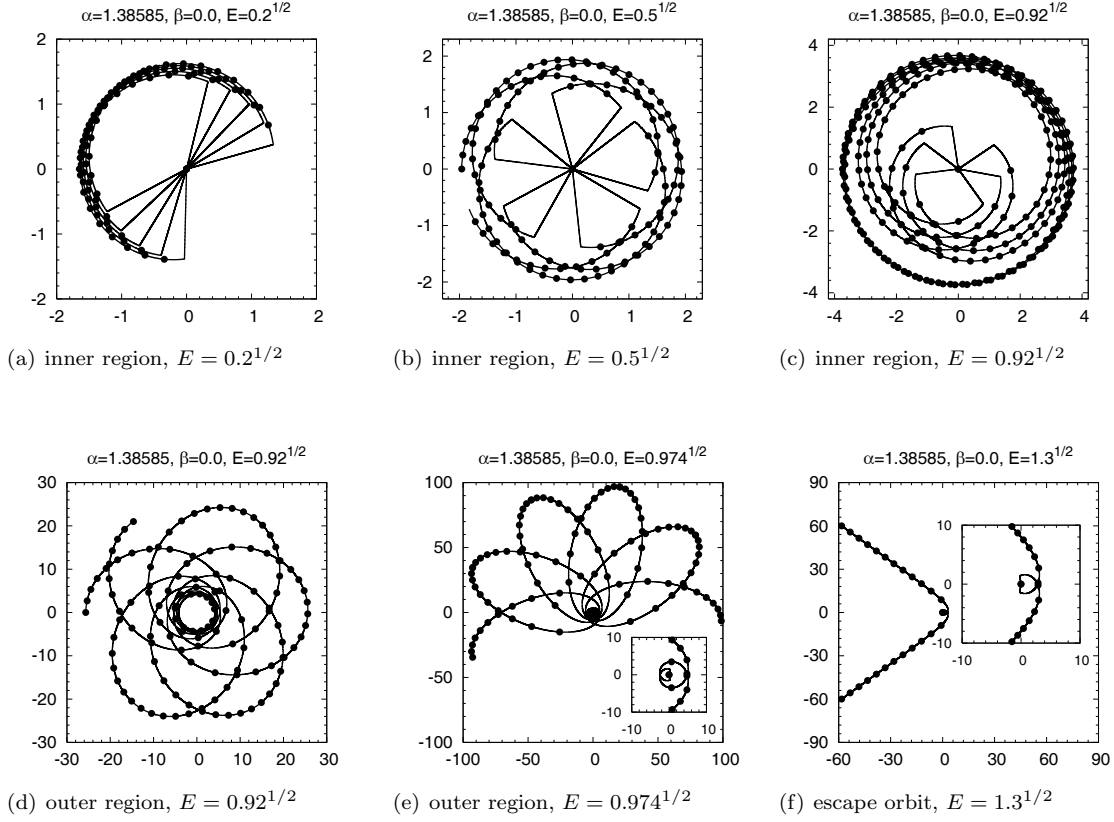


Figure 7: Particle orbits $r(\varphi)$ for $(\alpha_{\text{cr}}, \beta) = (1.38585, 0)$. The dots indicate units of elapsed proper time.

instead, since now the orbits are seen to move within the long throat of the space-time. This is demonstrated in Fig. 9 for the inner orbits of Fig. 6.

5.3 Orbits for $\beta > 0$

Let us now consider the effect of a finite value of the parameter β and thus the Higgs mass on the monopole space-times and consequently on the orbits in these space-times.

As β increases α_{max} decreases. At the same time, α_{cr} and α_{max} approach each other, until they merge. The critical space-time then arises at the maximal possible value of α for the given value of β . We exhibit such an *almost* critical space-time at $(\alpha, \beta) = (0.9, 4.49088)$ and study its orbits.

As β increases further another interesting phenomenon arises: $1/g_{rr}$ develops two minima. We study the evolution of such space-times towards the corresponding critical space-time at $(\alpha, \beta) = (0.85, 8.282558)$. We discuss the effects on the orbits of particles, and we exhibit orbits of light rays.

5.3.1 Orbits at $\alpha = 0.9$, $\beta = 4.49088$

We now address motion in an *almost* critical space-time at a finite, but still small value of β , namely at $\beta = 4.49088$. This value of β is obtained, by fixing $\alpha = 0.9$ and then increasing β , until $\alpha = 0.9$ becomes the maximal and at the same time critical value, $\alpha_{\text{max}} = \alpha_{\text{cr}} = 0.9$, i.e., for this specific value $\beta = 4.49088$ no regular solutions exist beyond $\alpha = 0.9$.

We exhibit the metric coefficients of this *almost* critical space-time in Fig. 10. The evolution of the monopole space-time towards the critical solution is similar the one discussed in the previous case, $(\alpha, \beta) = (1.38585, 0)$. As $\alpha \rightarrow \alpha_{\text{cr}}$ the minimum of the metric function $1/g_{rr}$ decreases and reaches zero in the limit.

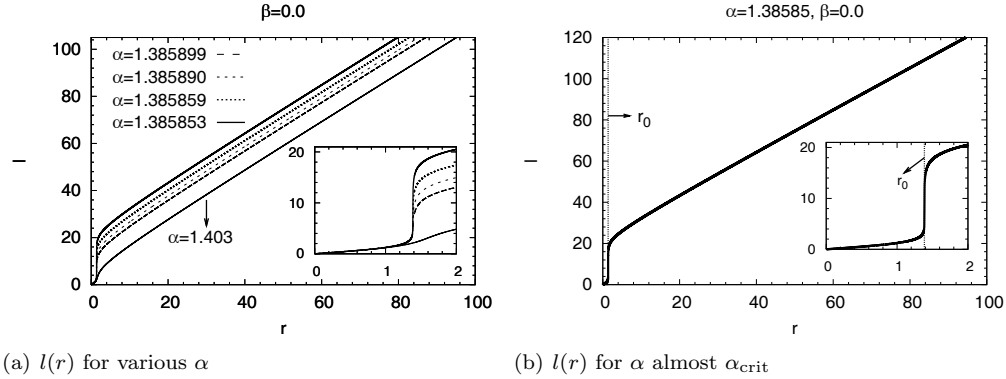


Figure 8: The measured spatial distance l versus the radial coordinate r . As α approaches α_{crit} a throat develops at $r = r_0$.

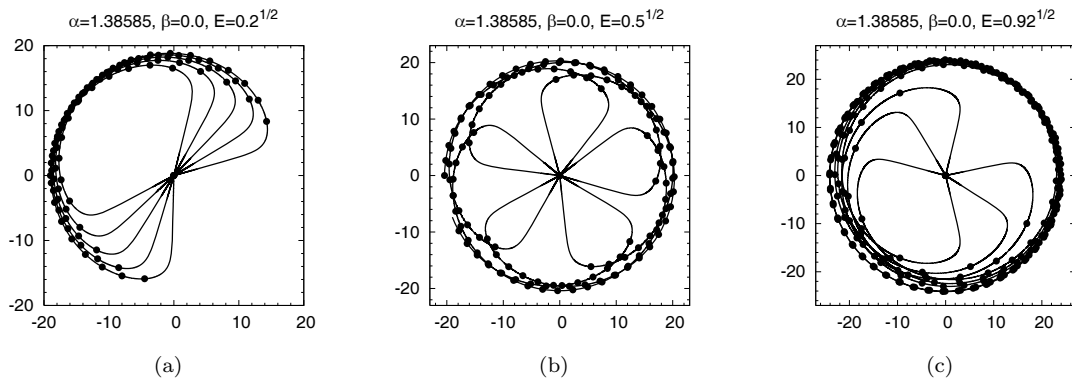


Figure 9: Particle orbits $l(\varphi)$ for $(\alpha_{\text{cr}}, \beta) = (1.385853, 0)$. The dots indicate units of elapsed proper time.

The true limiting solution then consists of the non-Abelian interior solution in the region $0 \leq r < r_0$, and the extremal Reissner–Nordström solution with degenerate horizon at $r_0 = \alpha$ in the exterior region $r_0 < r < \infty$.

Again, the metric function $-g_{tt}$ becomes increasingly small in the inner region, $0 \leq r < r_0$, as $\alpha \rightarrow \alpha_{\text{cr}}$, and rises very steeply in the vicinity of r_0 . The main difference to the previous case is, that $-g_{tt}$ is no longer monotonic, but that it has a minimum close to r_0 , before the steep rise. (Note, that this minimum foreshadows the appearance of a second minimum in g_{rr} for still larger values of β , discussed below.) In the limit $\alpha \rightarrow \alpha_{\text{cr}}$, $-g_{tt}$ again appears to become singular at r_0 , as reflected in Fig. 10 by the Kretschmann scalar.

Considering the motion of particles in the *almost* critical space–time, we again select for the angular momentum the value $L = 4.3$. The potential U then again possesses two minima, giving rise to similar orbits as observed in the previous case.

We display a set of characteristic orbits in Fig. 11. At very low energy (a) we observe smooth bound orbits in the inner region, which are limited by a circle at r_0 , that appears to form an outer envelope for the motion. As the energy increases, the bound orbits in the inner region (b) and (c), are again hugely distorted, exhibiting smooth segments alternating with almost straight radial lines.

The energy for the bound orbit in (b) is chosen, so that the motion is still limited by the circle at r_0 , but that the motion now either (almost) proceeds on segments of that circle or that it proceeds on almost straight radial lines to and from the center (with some reflection there).

The particle motion is again understood by examining the effective potential. As before, the abrupt changes in the motion followed by the straight radial line segments are caused by the extreme decrease of the effective potential in the region $r < r_0$, leading to vigorous attraction for the particle towards the origin. At the same time the particle needs almost no proper time to traverse the inner region.

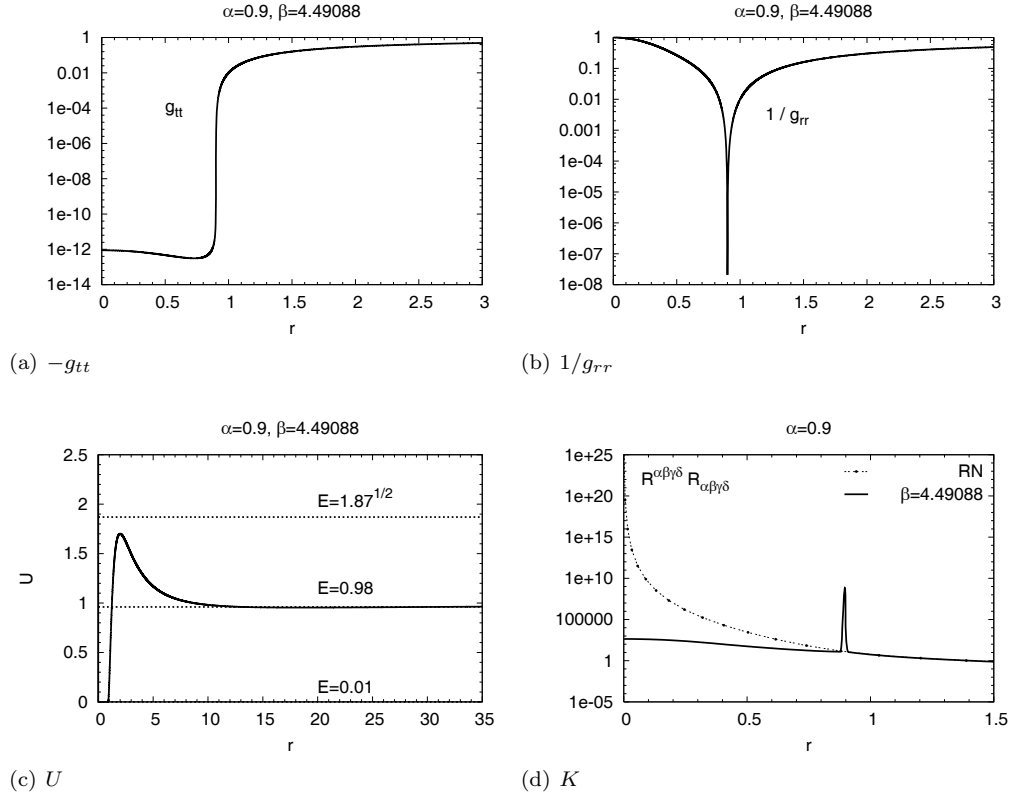


Figure 10: The metric functions $-g_{tt}$ (a) and $1/g_{rr}$ (b), the potential U (c), and the curvature invariant K (d) versus the radial coordinate r for $(\alpha, \beta) = (0.9, 4.49088)$. (RN denotes the extremal Reissner–Nordström black hole.)

Fig. 10 also exhibits a bound orbit in the outer region (d), and a scattering state (e). This scattering orbit reflects the maximum of the potential, when the particle traverses the inner loops circling the center, as well as the critical value r_0 , since the particle passes also the associated straight radial line segments close to the center.

5.3.2 Orbits at $\alpha = 0.85$, $\beta = 8.282558$

As our last example for motion in the space–time of a gravitating monopole, we discuss a case with intermediate Higgs mass, choosing the parameter set $(\alpha, \beta) = (0.85, 8.282558)$. Here a new phenomenon arises: the limiting space–time no longer corresponds to an extremal Reissner–Nordström solution in the exterior, but it retains non-Abelian fields there, which affect the features of the space–time [13].

Let us first consider, how the monopole space–time evolves in this case as the critical solution is approached. As in the last example, we fix α and increase β , until the *almost* critical space–time is reached. As $\beta \rightarrow \beta_{\text{cr}}$ (or analogously as $\alpha \rightarrow \alpha_{\text{cr}}$) the minimum of the metric function $1/g_{rr}$ close to $r_0 = \alpha$ decreases, but it does not reach zero. Instead, at a certain value of the parameter a second minimum appears at a value $r^* < r_0$. As the parameter is further evolved towards its critical value, it is this new minimum at r^* , which reaches zero in the limit, as anticipated from Fig. 12. The old minimum at r_0 is no longer affected by the final approach towards the critical solution.

The true limiting solution thus divides space–time in a different way and consists of the interior region $0 \leq r \leq r^*$ and the exterior region $r^* \leq r < \infty$, where the exterior region may be subdivided into the intermediate region $r^* \leq r < r_0$ and the outer region $r_0 < r < \infty$. Clearly, the metric of the limiting solution differs now from the metric of an extremal Reissner–Nordström black hole also in the exterior region of the limiting space–time $r^* \leq r < \infty$. Though for $r_0 < r < \infty$ it is still close to an extremal Reissner–Nordström space–time for the chosen parameters.

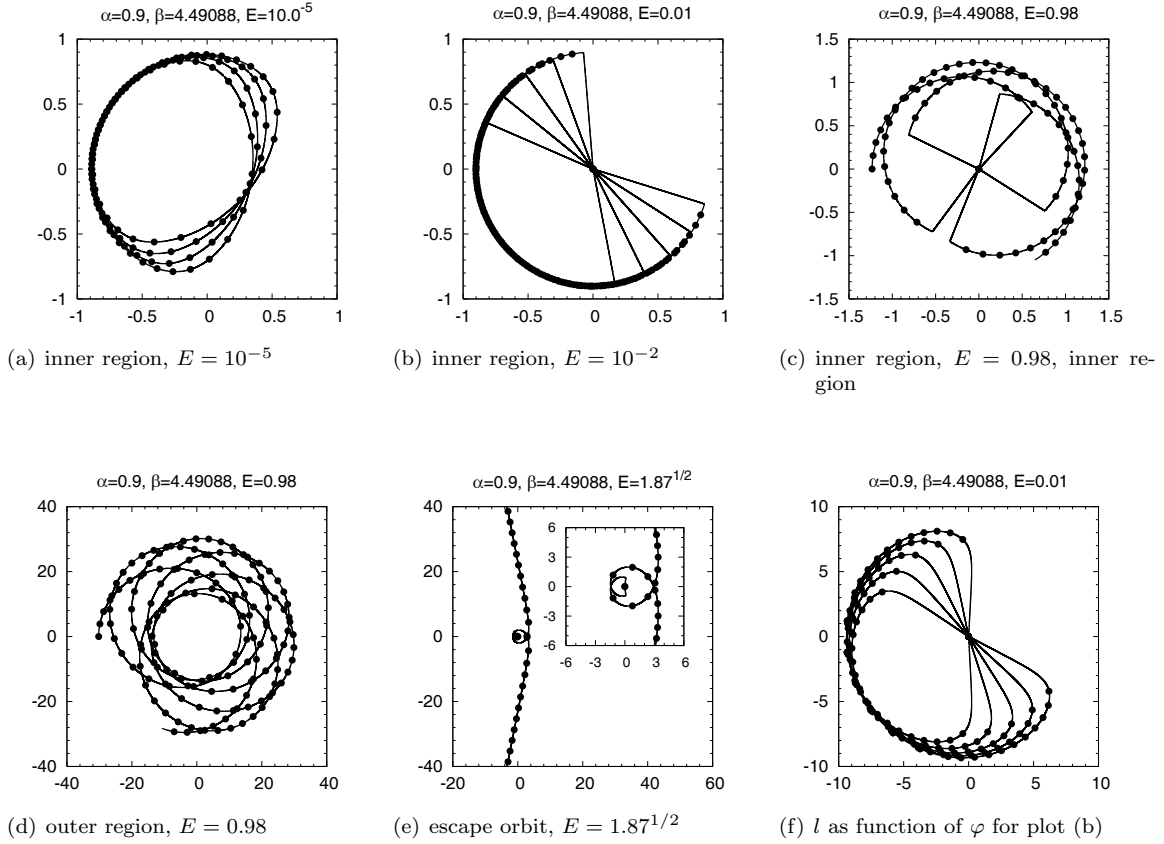


Figure 11: Particle orbits (a)-(e) $r(\varphi)$ and (f) $l(\varphi)$ for $(\alpha, \beta) = (0.9, 4.49088)$. The dots indicate units of elapsed proper time.

As in the case above with a single minimum at r_0 , the metric function $-g_{tt}$ becomes very small in the region $0 \leq r < r_0$, when $\beta \rightarrow \beta_{\text{cr}}$. However, unlike that case, it decreases distinctly faster at r^* than in the overall region $0 \leq r < r_0$. Thus $-g_{tt}$ develops a minimum at r^* quite analogous to the minimum of $1/g_{rr}$. As a consequence, the product of $-g_{tt}$ and g_{rr} changes only slightly in the vicinity of r^* , while, in contrast, $-g_{tt}g_{rr}$ changes very rapidly in the vicinity of r_0 .

The implication for the curvature of the space-time is, that there appears no singularity at r^* . The Kretschmann scalar remains perfectly smooth there, as seen in Fig. 12. On the other hand, the Kretschmann scalar still becomes very large at r_0 , but it will not diverge there in the limit. The critical space-time is thus expected to correspond to a space-time with a degenerate black hole horizon at r^* , and with no singularities at either r_0 or at the origin.

Let us now address the orbits of particles and also of light rays in this *almost* limiting space-time. We again choose for the angular momentum the previous value $L = 4.3$. The corresponding potential U is seen in Fig. 12.

Time-like geodesics

We display a set of characteristic particle orbits in Fig. 13. Since r^* is a minimum of g_{tt} the potential U also exhibits a minimum at r^* (the L^2 term is negligible here). For a very small minimal energy this implies an almost circular motion at r^* , exhibited in (a). The associated effective potential U_{eff} (Fig. 12 (f)) also assumes its minimal value at r^* .

As the energy is increased, the effective potential changes drastically and rapidly assumes huge negative values in the region bounded by r_0 (and not only the region bounded by r^*). Thus r_0 still plays a most significant role for the orbits. For instance, the energy for the bound orbit in (b) is again chosen, such that the motion is limited by the circle at r_0 . The motion then proceeds either on segments of that circle or on

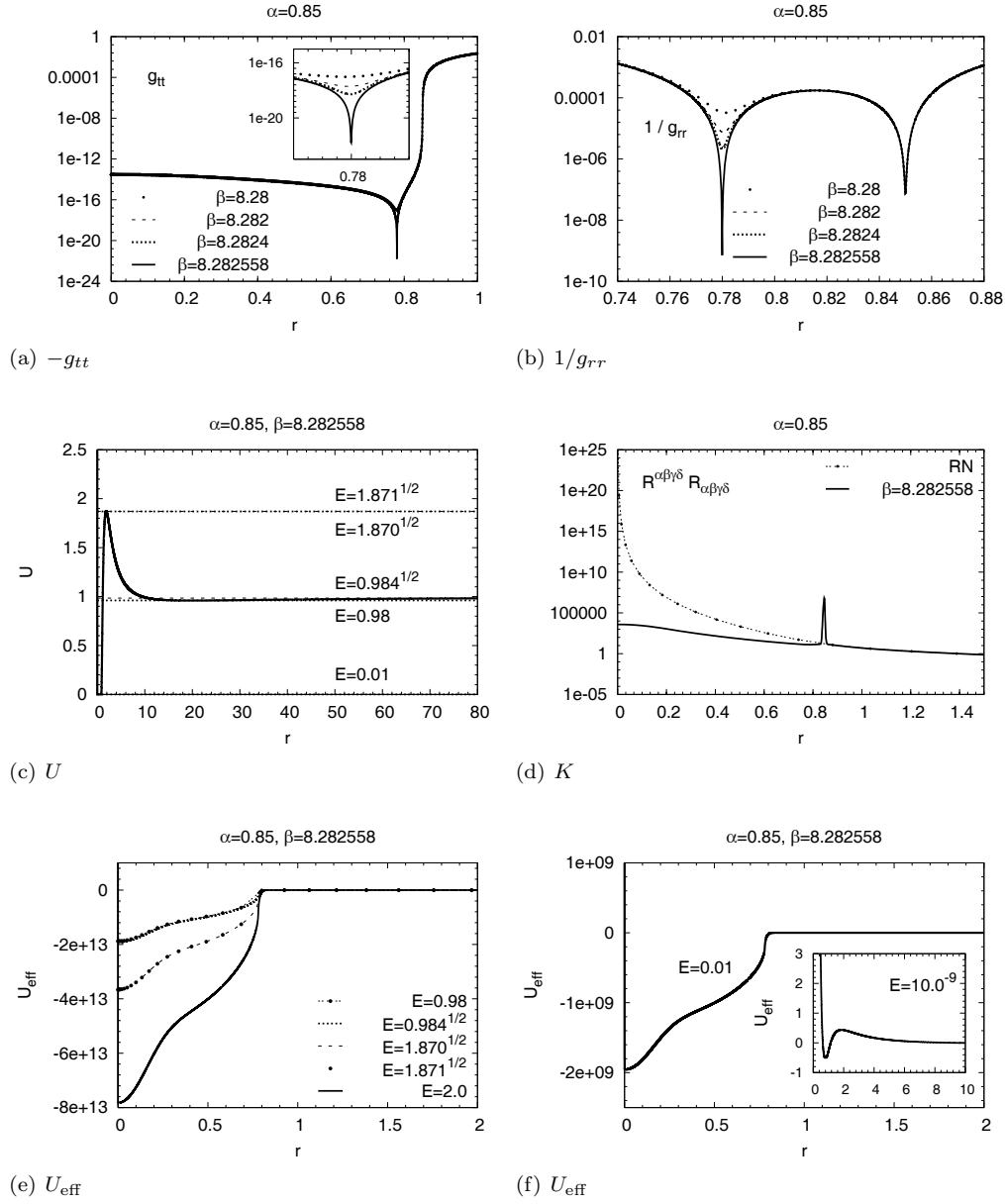


Figure 12: The metric functions $-g_{tt}$ (a) and $1/g_{rr}$ (b), the potential U (c), and the curvature invariant K (d), the effective potential U_{eff} (e) and (f), versus the radial coordinate r for $(\alpha, \beta) = (0.85, 8.282558)$. (RN denotes the extremal Reissner-Nordström black hole.)

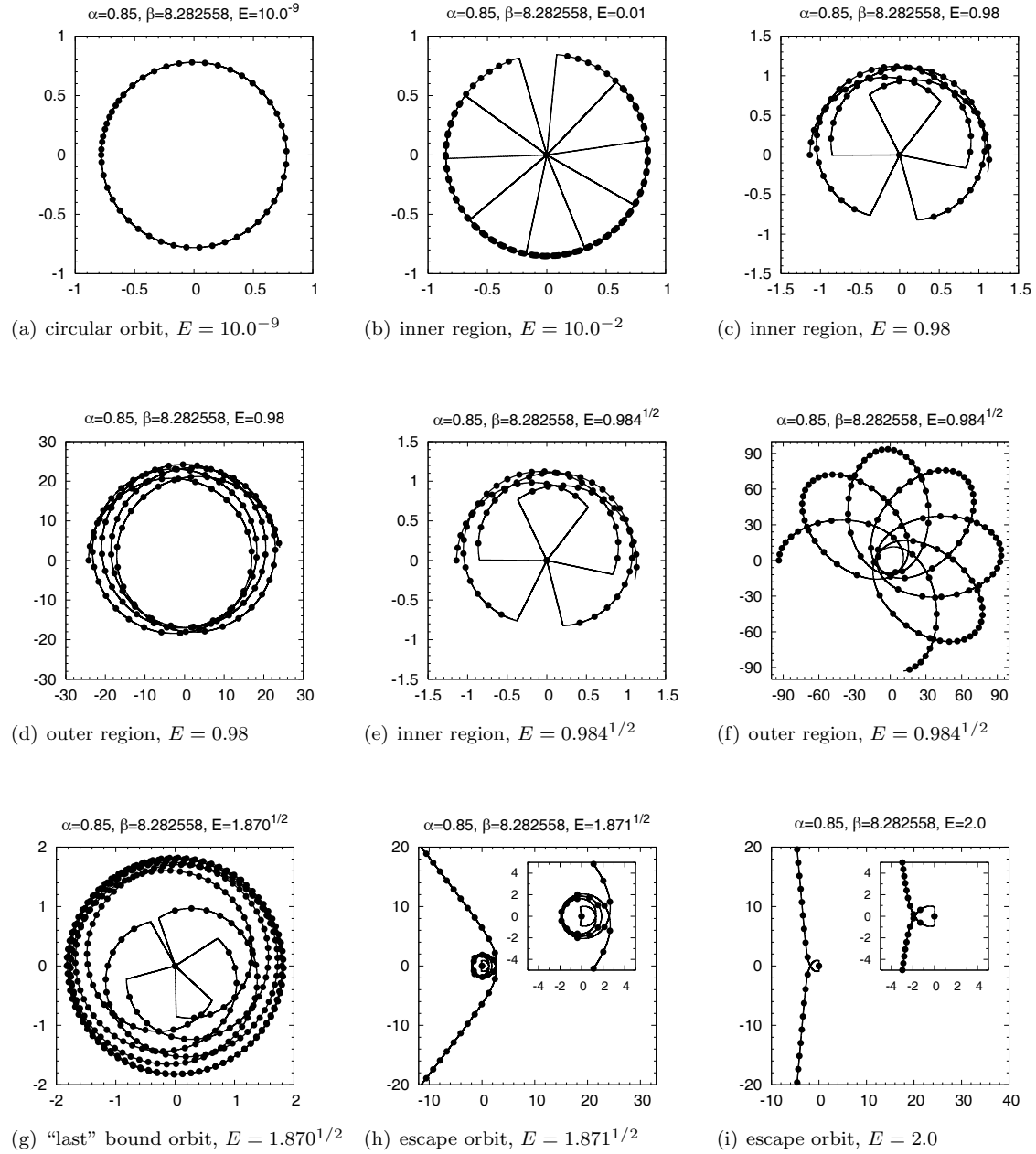


Figure 13: Particle orbits $r(\varphi)$ for $(\alpha, \beta) = (0.85, 8.282558)$. The dots indicate units of elapsed proper time.

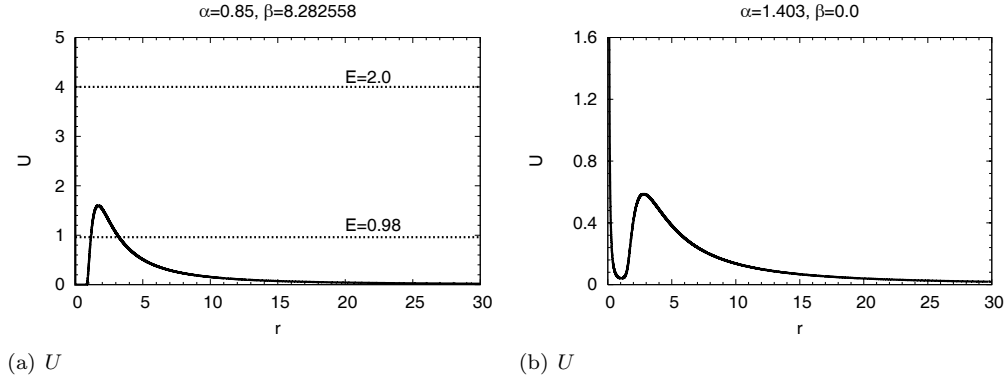


Figure 14: The potential U for null geodesics versus the radial coordinate r for $(\alpha, \beta) = (0.85, 8.282558)$, as well as for $(\alpha, \beta) = (1.403, 0)$ (subsection 5.2.2).

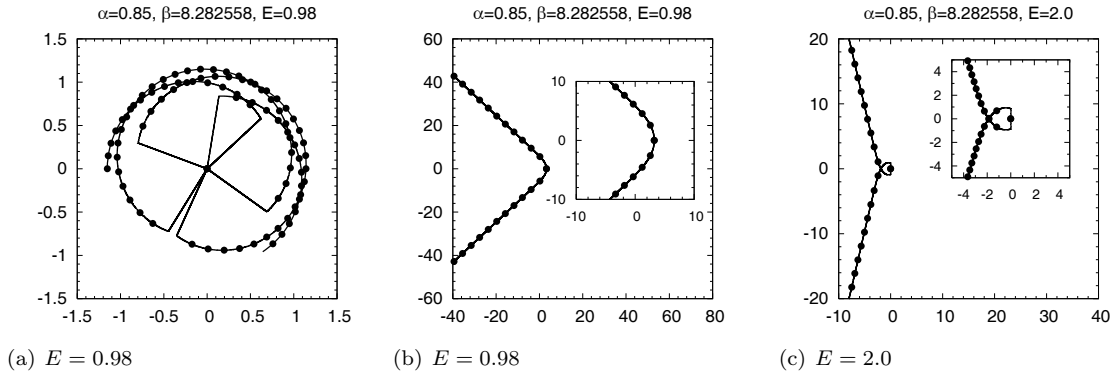


Figure 15: Null geodesics $r(\varphi)$ for $(\alpha, \beta) = (0.85, 8.282558)$.

almost straight radial lines to and from the center (with some reflection there).

At somewhat higher energies the bound orbits in the inner region (c) and (e) again exhibit smooth segments which alternate with almost straight radial lines to and from the center, where the abrupt directional changes occur at r_0 (and at the center). This remarkable role of r_0 is preserved also in the weakly bound orbits (g) and in the escape orbits (h) and (i). As discussed above, a particle needs very little proper time to traverse the inner region.

The bound orbits in the outer region (d) and (f), of course, do not penetrate far enough inside to experience any influence of r_0 . These trajectories are ordinary quasi-elliptic orbits with a perihelion shift.

Null geodesics

We have also considered the null geodesics in this space-time. The potential U for light rays ($\epsilon = 0$) is shown in Fig. 14, while a set of orbits is exhibited in Fig. 15. The null geodesics are interesting due to the fact, that light rays can follow bound geodesics, as evident from the form of the potential U . Thus light can be captured by the source, but does not fall into any singularity, since the space-time is regular.

The shape of the null geodesics is similar to the shape of the time-like geodesics, as seen in Fig. 15. The bound orbits (a) again exhibit smooth segments which alternate with almost straight radial lines to and from the center, with abrupt directional changes at r_0 (and at the center), related to the fact that the effective potential becomes very large and negative in the region within the radius r_0 . This peculiar effect on the motion at and within radius r_0 is also seen in the scattering orbits at high enough energy (c). The scattering orbits at lower energy (b) are deflected before they can experience any influence of r_0 .

6 Conclusions and outlook

An accurate analysis and true interpretation of a given gravitational field can only be obtained through the exploration of the geodesics of particles and light rays in this space–time. Such an investigation is particularly important in regions, where the space–time metric exhibits unusual behavior, as for example in the vicinity of a black hole event horizon.

In this paper we have discussed the motion of particles and light rays in the gravitational field of a magnetic monopole which is characterized by two dimensionless constants, α and β , where α signifies the relative strength of gravity, while β is the ratio of the Higgs boson to the vector boson mass in the non-Abelian gauge theory.

The space–time of a non-Abelian monopole is globally regular. Its curvature invariants are finite everywhere. However, globally regular monopoles cannot exist for large values of the gravitational coupling strength. Simple dimensional reasoning shows, that black holes should form, when α reaches values on the order of one [6]. Indeed, at critical values of the parameters $(\alpha_{\text{cr}}, \beta_{\text{cr}})$ the space–time changes dramatically and the metric becomes singular.

As the critical space–time is approached for small values of β , the metric coefficient $1/g_{rr}$ tends to zero at $r_0 = \alpha_{\text{cr}}$, and the metric coefficient g_{tt} tends to zero in the interval $0 < r < r_0$. The effects on the particle orbits are then astounding. The orbits traversing the region, where r_0 is located, are hugely distorted as compared to ordinary bound orbits. While the orbits evolve smoothly until they reach the vicinity of r_0 , they then change abruptly direction and approach the center in almost straight radial lines. There they are reflected, and move in almost straight radial lines out to r_0 , where they change abruptly direction again and evolve smoothly further. This intriguing pattern of movement is caused by the steep drop of the effective potential for $r < r_0$, leading to a vigorous attraction of particles or light rays in this region. Also, particles need almost no proper time to traverse this region ($r < r_0$).

For larger values of β , the critical space–time is distinctly different [13]. The metric coefficient $1/g_{rr}$ acquires a second minimum at $r^* < r_0$, which tends to zero in the limit, while the minimum at r_0 remains finite. Still it is r_0 , and the steep drop of the effective potential associated with it, which strongly dominates the orbits in the interior, causing abrupt directional changes and vigorous attraction towards the center, along with almost no lapse of proper time.

We note, that this kind of research may be extended to metrics associated with stationary axially symmetric solutions of the Einstein field equations. There are interesting examples where counterrotating horizons appear [14] or negative horizon masses [15]. Such unusual features of various space–times may be explored best through the study of the motion of particles and light. This may be extended to the study of particles with spin [16].

Another extension of the present considerations is the study of the motion of satellites and stars in the gravitational field of a modified gravitational theory. This may have applications to the Pioneer anomaly, the flyby anomaly, or the increase of the astronomical unit [17], which are all problems which are unresolved within standard general relativity.

Acknowledgement

We would like to thank P. Breitenlohner, B. Kleihaus, and D. Maison for valuable discussions. V.K. thanks the German Academic Exchange Service DAAD and C.L. the German Aerospace Center DLR for financial support.

References

- [1] J. Ehlers, *Gen. Rel. Grav.* **38** (2006) 1059.
- [2] Y. Hagihara, Theory of relativistic trajectories in a gravitational field of Schwarzschild, *Japan. J. Astron. Geophys.* **8** (1931) 67.
- [3] S. Chandrasekhar, *The Mathematical Theory of Black Holes* (Oxford University Press, Oxford 1983).
- [4] Y. Hagihara, Y., *Celestial Mechanics* (MIT Press, Cambridge, Mass., 1970).

- [5] G. 't Hooft, Nucl. Phys. **B79** (1974) 276;
A.M. Polyakov, Pis'ma JETP **20** (1974) 430.
- [6] K. Lee, V.P. Nair, and E.J. Weinberg, Phys. Rev. **D45** (1992) 2751;
P. Breitenlohner, P. Forgacs, and D. Maison, Nucl. Phys. **B383** (1992) 357;
P. Breitenlohner, P. Forgacs, and D. Maison, Nucl. Phys. **B442** (1995) 126.
- [7] R. Bartnik, and J. McKinnon, Phys. Rev. Lett. **61** (1988) 141.
- [8] see e.g. M. S. Volkov and D. V. Gal'tsov, Phys. Rept. **319** (1999) 1.
- [9] J.B. Hartle, *Gravity. An Introduction to Einstein's General Relativity* (Addison Wesley)
- [10] V.P. Frolov and I.D. Novikov, *Black Hole Physics* (Kluwer Academic Publishers, Dordrecht 1998)
- [11] V. Kagramanova, J. Kunz, and C. Lämmerzahl, in preparation.
- [12] C.W. Misner, K. Thorne, and J.A. Wheeler, *Gravitation* (Freeman, San Francisco 1973).
- [13] A. Lue and E.J. Weinberg, Phys. Rev. **D60** (1999) 084025;
P. Breitenlohner, P. Forgacs, and D. Maison, in preparation.
- [14] B. Kleihaus, J. Kunz, and F. Navarro-Lérida, Phys. Rev. **D69** (2004) 081501;
J. Kunz, and F. Navarro-Lérida, Phys. Rev. Lett. **96** (2006) 081101;
J. Kunz, and F. Navarro-Lérida, Mod. Phys. Lett. **A21** (2006) 2621.
- [15] J. Kunz, and F. Navarro-Lérida, Phys. Lett. **B643** (2006) 55;
M. Ansorg, and D. Petroff, Class. Quant. Grav. **23** (2006) L81.
- [16] C. Chicone, B. Mashhoon, and B. Punsly, Phys. Lett. **A 343** (2005) 1.
- [17] C. Lämmerzahl, O. Preuss, and H. Dittus, Is the physics in the Solar System really understood? in H. Dittus, C. Lämmerzahl, and S.G. Turyshev (eds.) *Lasers, Clocks, and Drag-Free Control: Exploration of Relativistic Gravity in Space*, (Springer-Verlag, Berlin 2007).